Journal of Structural Geology 30 (2008) 1300–1313

Contents lists available at ScienceDirect

Journal of Structural Geology

journal homepage: www.elsevier.com/locate/jsg

Mass transfers and volume changes related to pressure solution–fracturing interactions in carbonate rocks: Example of the Oligocene deformation of the Coniacian chalk from the Omey area (Paris Basin, France)

J. Richard*

U.M.R. 6249 Chrono-environnement, Département de Géosciences, U.F.R. Sciences et Techniques, Université de Franche-Comté, 16 route de Gray, 25030 Besançon Cedex, France

ARTICLE INFO

Article history:
Received 19 March 2008
Received in revised form 11 July 2008
Accepted 14 July 2008
Available online 25 July 2008

Keywords:
Deformation
Pressure solution
Mass transfer
Fracture
Diagenesis
Carbonate

ABSTRACT

The present contribution documents the interactions between pressure solution and fracturing in carbonate rocks by studying the mass and volume changes caused by the Oligocene deformation of the Coniacian chalk from the Omey area. The isocon method allowed to establish that the decreases in interstitial fluid pressure resulting from the development of one normal fault and related tension gashes within a 11.4 m wide zone induced mass and volume changes within a 30.2 ± 3.5 m wide zone. In the hangingwall as well as in the footwall, the deformed zones adjacent to the fault plane exhibit mass gains (up to 58%) while the outermost deformed zones show mass losses (up to 36%). The pressure solution–fracturing interactions caused a mass redistribution from the most porous zones (outermost deformed zones) to the least porous zones (deformed zones adjacent to the fault plane) linked to differences in stress–strain energy of grain aggregates. The mass transfers strongly controlled the volume changes. Chemical compaction occurred only within the outermost deformed zones where mass losses took place in response to the reduction in solid–solid contacts. The zones affected by chemical compaction show equal mass and volume losses.

1. Introduction

Pressure solution (fluid-enhanced deformation) is considered to be a major mechanism of rock deformation. In the upper crust, pressure solution often plays an important role within zones where it is spatially associated with brittle deformation (Gratier et al., 1999). Therefore, it is crucial to examine how these two mechanisms of deformation, operating at two time scales, interact in order to better understand the complex mechanical behaviour of the upper crust.

Several contributions have focussed on the interactions between pressure solution and fracturing processes by studying natural or experimental deformation in carbonates (Mimran, 1975, 1977; Jones et al., 1984; Carrio-Schaffhauser and Gaviglio, 1990; Gaviglio et al., 1993, 1997, 1999; Richard et al., 2002; Hellmann et al., 2002a,b; Angelier et al., 2006). These studies have provided important data about the pressure solution–fracturing interactions in carbonates rocks but the mass and volume changes due to these mechano-chemical interactions were poorly documented. The present contribution attempts to document these mass and volume changes by studying the Oligocene deformation of the Coniacian chalk from the Omey area (eastern part of the Paris Basin). Previous works (Richard et al., 1997, 1999, 2002) highlighted the interest of this case study in order to examine the interactions between pressure solution and fracturing processes in carbonate rocks. The purpose of this paper is (1) to quantify the mass transfers and volume changes caused by the development of one normal fault and related tension gashes within a 11.4 m wide zone, (2) to determine the spatial distribution of these mass transfers and volume changes, (3) to examine the relationships between the mass and volume changes and fracturing, and (4) to propose a physico-chemical model of the deformation mechanism.

2. Geological setting

An extensional stress field associated with the development of the West-European Rift affected the West-European Platform during the Oligocene (Bergerat, 1987a,b; Coulon and Frizon de Lamotte, 1988a; Coulon, 1992). In the eastern part of the Paris Basin, this extension led to the formation of the Mayence-Sancerre Fault Zone (Coulon, 1992; Fig. 1).

In the Omey area, the chalk is fractured in a 6-km wide N060°E zone which follows the trace of the Omey Fault, the northern border of the Mayence–Sancerre Fault Zone (Coulon and Frizon de

* Tel.: +33 3 81 66 64 34; fax: +33 3 81 66 65 58.
E-mail address: james.richard@univ-fcomte.fr

0191-8141/$ – see front matter © 2008 Elsevier Ltd. All rights reserved.
doi:10.1016/j.jsg.2008.07.003

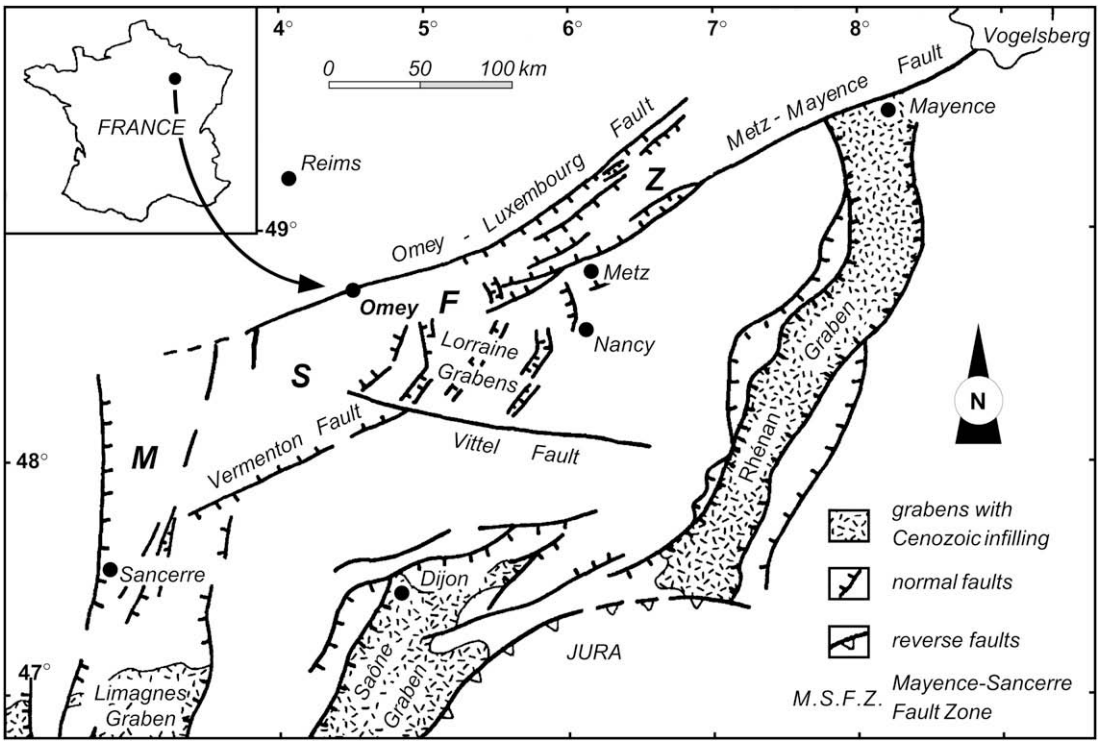

Fig. 1. Structural map of the eastern part of the Paris Basin (modified after Coulon, 1992) showing the Mayence–Sancerre Fault Zone (M.S.F.Z.) resulting from the Oligocene extensional stress field associated with the development of the West-European Rift.

Lamotte, 1988b; Coulon, 1992; Figs. 1 and 2). In this area, the Oligocene extension reactivated a basement fault that led to the development of normal faults and tension gashes at depths estimated between −150 and −250 m (Coulon and Frizon de Lamotte, 1988a,b; Coulon, 1992). These fractures grew in an unconfined phreatic zone where the interstitial fluid was meteoric (Richard et al., 1999).

3. Sampling, methods and analytical techniques

3.1. Sampling

Sixty samples of Coniacian chalk were collected along a 100 m wide working face (Fig. 3A) in the Marson Quarry (Fig. 2). This outcrop shows a 11.4 m wide fractured zone with one normal fault

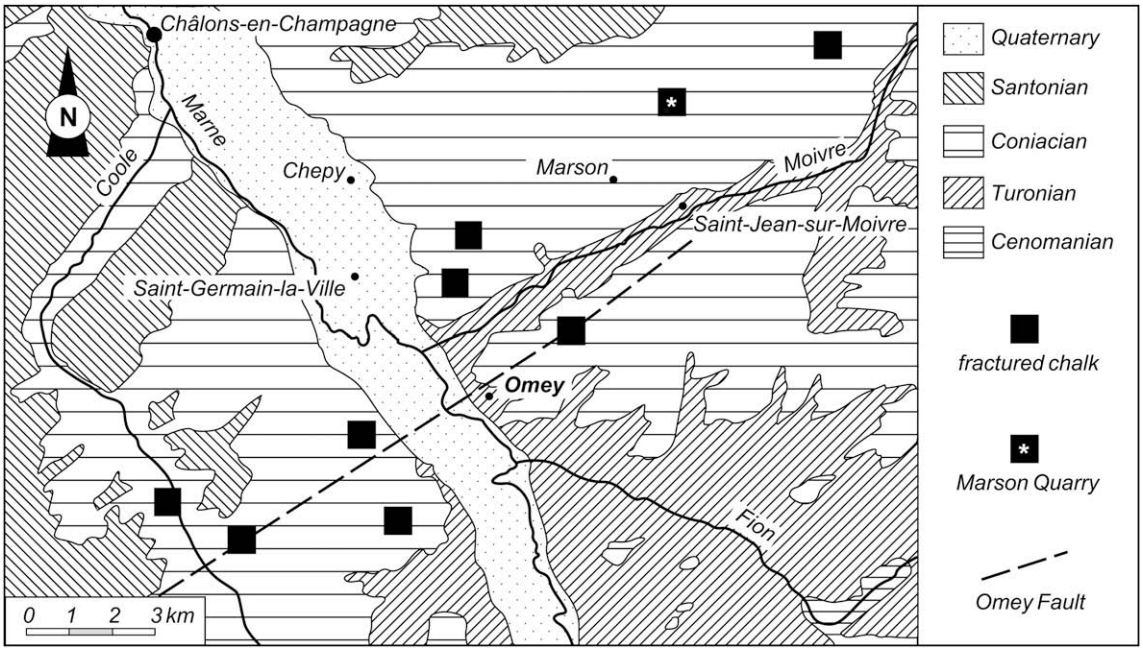

Fig. 2. Geological map of the Omey area with location of the Marson Quarry (modified after Coulon and Frizon de Lamotte, 1988b). The chalk is fractured in a 6-km wide N060°E zone which follows the trace of the Omey Fault (northern border of the Mayence–Sancerre Fault Zone).

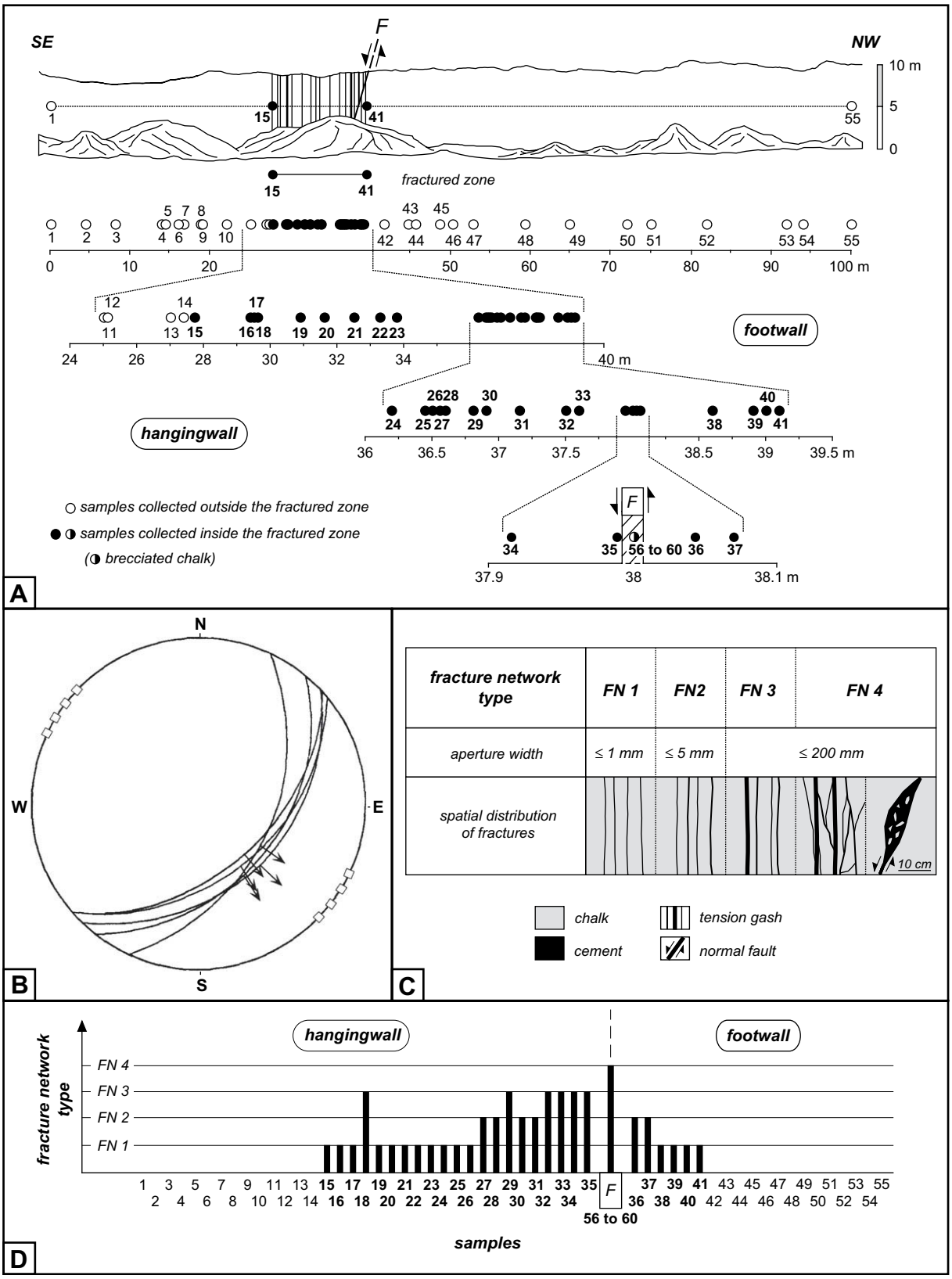

Fig. 3. (A) Sketch of the studied working face with location of collected samples. (B) Stereographic projection of the normal fault plane *F*, the striation lineations borne by *F* and the poles to tension gashes (white squares). (C) Four fracture network types (FN 1, 2, 3 and 4) can be distinguished by using the aperture width and the spatial distribution of fractures. (D) Fracture network type of the 60 sampling points.

and tension gashes filled by calcite cements (Fig. 3A,B). Four fracture network types can be distinguished along the working face by using the aperture width and the spatial distribution of fractures (Fig. 3C):

- FN 1: weakly fractured zone with subvertical and irregularly spaced tension gashes which show an aperture width ≤1 mm;
- FN 2: moderately fractured zone with subvertical and irregularly spaced tension gashes which display an aperture width ≤5 mm;
- FN 3: strongly fractured zone with subvertical and irregularly spaced tension gashes which present an aperture width ≤200 mm;
- FN 4: very strongly fractured zone showing subvertical, irregularly spaced and connected tension gashes which show an aperture width ≤200 mm or brecciated chalk located along the fault plane.

The fracture network type of the 60 sampling points is given in Fig. 3D.

3.2. Mass and volume changes: method

Isocon method is an effective means of quantitatively evaluating changes in volume and mass in a wide range of geological processes (Grant, 1986, 2005). In the isocon analysis, the Gresens' equation (Gresens, 1967) was rewritten as:

$$C_i^A = M^O/M^A\left(C_i^O + \Delta C_i\right) \quad (1)$$

where C_i^O and C_i^A are the concentrations of the major or trace element i in the original and altered rock respectively, M^O and M^A are the masses of the original and altered rock respectively and ΔC_i denotes the change in concentration of the major or trace element i between the original and altered rock. For an immobile element, the equation (1) can be written:

$$C_i^A/C_i^O = M^O/M^A = 1 \quad (2)$$

because $\Delta C_i = 0$. The masses of the original and altered rock (M^O and M^A respectively) can be expressed by the formulae:

$$M^O = \rho^O V^O \quad (3)$$

$$M^A = \rho^A V^A \quad (4)$$

where ρ is the bulk density and V the volume. Combining the equation (2) with the equations (3) and (4), we can write:

$$C_i^A/C_i^O = M^O/M^A = \left(\rho^O V^O\right)/\left(\rho^A V^A\right) = 1 \quad (5)$$

Equation (5) allows calculation ofthe changes in volume and mass by using the analytical data C_i^O, C_i^A, ρ^O and ρ^A:

$$V^O/V^A = \left(C_i^A/C_i^O\right)\left(\rho^A/\rho^O\right) \quad (6)$$

$$M^O/M^A = \left(\rho^O/\rho^A\right)\left(V^O/V^A\right) = C_i^A/C_i^O \quad (7)$$

V^O/V^A (or M^O/M^A) > 1 indicates a volume (or mass) loss, V^O/V^A (or M^O/M^A) < 1 indicates a volume (or mass) gain, V^O/V^A (or M^O/M^A) $= 1$ indicates an alteration without change in volume (or mass). In this paper, the volume and mass changes are given in %.

3.3. Analytical techniques

3.3.1. Geochemical analyses

The concentrations of 53 elements were measured in SARM (Service d'Analyse des Roches et des Minéraux, Vandoeuvre-lès-Nancy, France) by:

- AAS (atomic absorption Perkin Elmer 5100): Si, Al, Fe, Mn, Mg, Ca and Na;
- ICP-MS (mass spectrometer Perkin Elmer 5000): As, Ba, Be, Bi, Cd, Ce, Co, Cr, Cs, Cu, Dy, Er, Eu, Ga, Gd, Ge, Hf, Ho, In, La, Lu, Mo, Nb, Nd, Ni, Pb, Pr, Rb, Sb, Sm, Sn, Sr, Ta, Tb, Th, Tm, U, V, W, Y, Yb, Zn and Zr;
- absorptiometry (spectrophotometer Beckman DU62): Ti and P.

The samples were ground to fine powders in an agate ball mill. The subsamples were fused with lithium metaborate and the melts dissolved in acid solutions. The concentrations are expressed in parts per million (ppm). In the concentration ranges observed in this study, the analytical accuracy is:

- <5% for Ca, Eu, Gd, La, Nd, Sr, Tb and Y;
- <10% for Al, Ba, Ce, Dy, Er, Ho, K, Lu, Mg, Mn, Na, Pb, P, Pr, Si, Sm, U and Yb;
- <15% for Co, Nb, Rb, Th, Zn and Zr;
- <20% for Fe;
- >25% for Ga, Hf, Ni, Ta, Tm and V.

The carbon and oxygen isotope analyses were carried out in the Institute of Geology of Bern University (Switzerland) using a VG Prism II mass spectrometer. The samples were ground to fine powders in an agate ball mill. The samples were dissolved in H_3PO_4 at 90 °C. All measurements were calibrated to the Pee Dee Belemnite (PDB) standard and the isotope ratios are given in the conventional δ-notation. The analytical accuracy is ±0.1‰ for $\delta^{18}O$ and ±0.05‰ for $\delta^{13}C$.

3.3.2. Bulk density measurements

Water porosimetry measurements were performed to determine the bulk density. The samples were dried at 60 °C until they reached a stable mass (M_d). They were then degassed during 24 h in an airtight enclosure before being progressively saturated, from their bottom, with a degassed and distilled water under a dynamic vacuum. The bulk density (ρ) is given by the expression:

$$\rho = M_d/(M_1 - M_2)$$

where M_1 is the mass of the sample entirely saturated with a degassed and distilled water and M_2 is the mass of the underwater sample. The analytical accuracy is ±0.002.

4. Results

4.1. Geochemical signature of the deformation

4.1.1. Major and trace elements

The elemental signature of the deformation was clarified by studying 53 chemical elements. The concentrations of 15 elements (As, Be, Bi, Cd, Cr, Cs, Cu, Ge, In, Mo, Sb, Sn, Ta, Ti and W) are below detection limits. 25 elements show strong evidence of variations caused by the development of the studied fractured zone. The examination of concentration versus sample position curves and the correlation matrix from the normalised principal component analysis of the chemical data-set allow to distinguish 5 elemental signatures:

- *Sr* (Fig. 4): The Sr concentrations range between 367 ppm (lowest value, sample 35) and 738 ppm (highest value, sample 54). In the brecciated chalk (samples 56 to 60), the concentrations vary between 378 and 478 ppm (mean = 423 ppm). The Sr concentrations are depleted within a 30.2 ± 3.5 m wide zone (samples 9–10 to 45–47). The Sr-depleted zone is wider

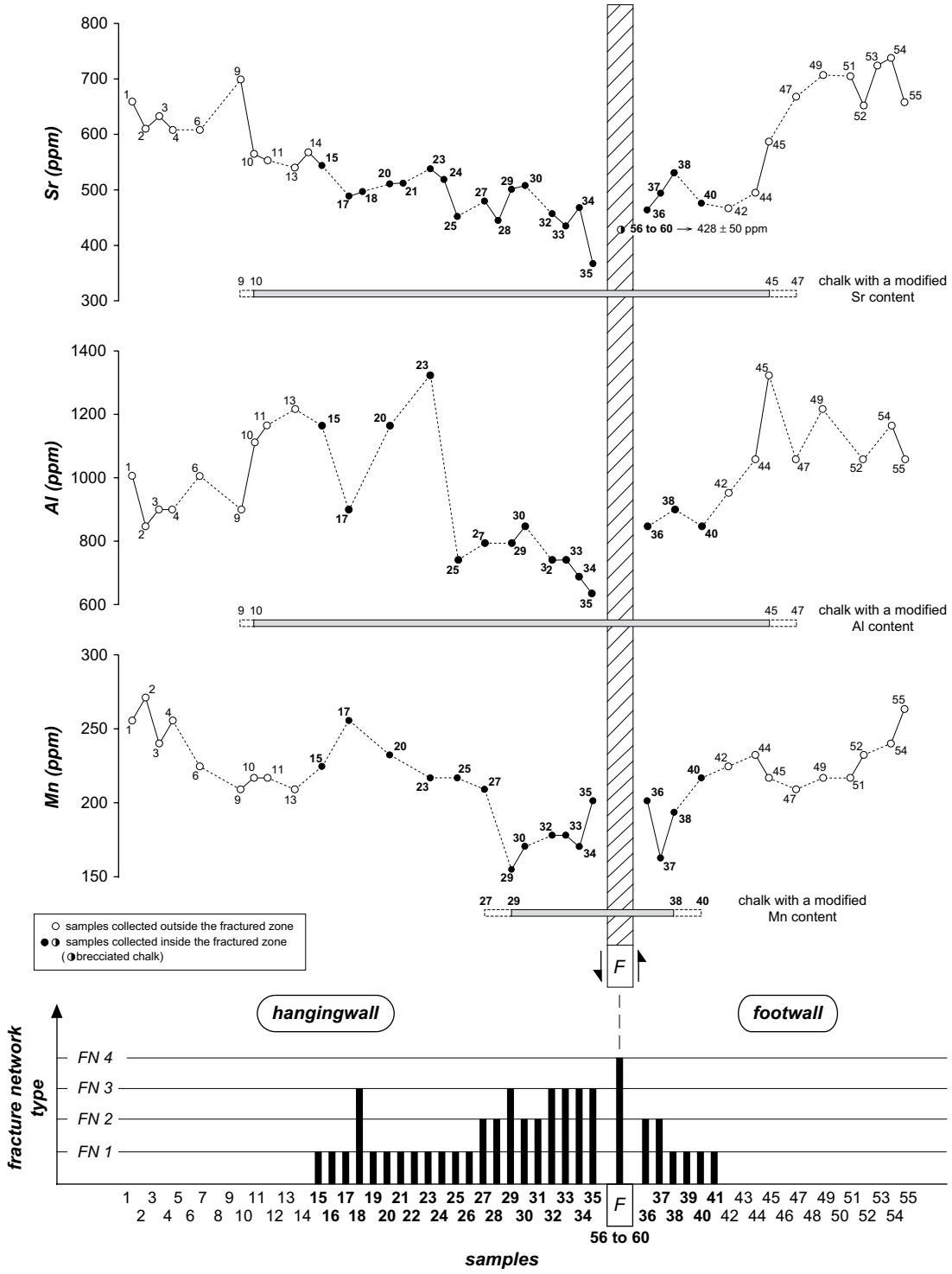

Fig. 4. Evolution of the elemental composition (Sr, Al and Mn) of the Coniacian chalk collected in the Marson Quarry along the studied outcrop. The chemical data are plotted by using a constant sampling interval on the *x*-axis.

than the fractured zone in the hangingwall as well as in the footwall.

– *Al, K, Rb, Si, Ta, Th, Y and rare earth elements*: These major and trace elements display the same behaviour. The Al concentration versus sample position curve (Fig. 4) allows description of this behaviour. The Al concentrations range between 635 ppm (lowest value, sample 35) and 1323 ppm (highest value, samples 23 and 45). In the hangingwall, the Al concentrations increase within an external zone (samples 10, 11, 13, 15, 20 and 23) where the chalk is not or weakly (FN 1) fractured and they decrease within an internal zone (samples 25, 27, 29, 30, 32 to 35) where the chalk is weakly (FN 1) to strongly (FN 3) fractured. In the footwall, an Al enrichment is observed within an external zone (sample 45) where the chalk is not fractured and an Al depletion is noticed within an internal zone (samples 36, 38, 40 and 42) where the chalk is not or weakly (FN 1) to moderately (FN 2) fractured. The Al content is modified within a 30.2 ± 3.5 m wide zone (samples 9–10 to 45–47). The

Al-modified zone is wider than the fractured zone in the hangingwall as well as in the footwall.

- *Mn* (Fig. 4): The Mn concentrations vary between 155 ppm (lowest value, sample 29) and 271 ppm (highest value, sample 2). Mn depletion is observed in both sides of the fault plane within a 2.1 ± 0.3 m wide zone (samples 27–29 to 38–40). In this Mn-depleted zone, samples 35 and 36 show the highest concentrations.
- *Fe* (Fig. 5): The Fe concentrations range between 406 ppm (lowest value, sample 9) and 3147 ppm (highest value, sample 35). Fe enrichment is observed near the fault plane within a 1.1 ± 0.6 m wide zone (samples 30–32 to 37–38);
- *Na* (Fig. 5): The Na concentrations vary between 97 ppm (lowest value, samples 33 and 34) and 171 ppm (highest value, samples 49 and 54). Na depletion is observed within a 23.7 ± 3 m wide zone (samples 10–11 to 44–45). The Na-depleted zone is wider than the fractured zone in the hangingwall as well as in the footwall.

Unlike rare earth element concentrations, the development of the fractured zone did not induce significant modifications in rare earth element pattern: all rare earth element patterns are similar in shape (Fig. 6). They are characterized by a distinct negative Ce anomaly and by a flat baseline reflecting a lack of fractionation between light, middle and heavy rare earth elements (Fig. 6).

4.1.2. Carbon and oxygen stable isotopes

$\delta^{13}C$ (Fig. 7): The $\delta^{13}C$ values range between $-2.07‰$ (lowest value, sample 35) and $2.79‰$ (highest value, sample 3). In the brecciated chalk (samples 56–60), the $\delta^{13}C$ values vary between -0.68 and $-0.30‰$ (mean $= -0.41‰$). A $\delta^{13}C$ depletion is observed within a 15.1 ± 1.9 m wide zone (samples 20–21 to 44–45). In the footwall, the $\delta^{13}C$-depleted zone is wider than the fractured zone.

$\delta^{18}O$ (Fig. 7): The $\delta^{18}O$ values range between $-3.86‰$ (lowest value, sample 35) and $-1.3‰$ (highest value, sample 18). In the brecciated chalk (samples 56 to 60), the $\delta^{18}O$ values vary between -3.49 and $-3.37‰$ (mean $= -3.43‰$). A $\delta^{18}O$ depletion is observed within a 18 ± 3.1 m wide zone (samples 20–23 to 45–47). In the footwall, the $\delta^{18}O$-depleted zone is wider than the fractured zone.

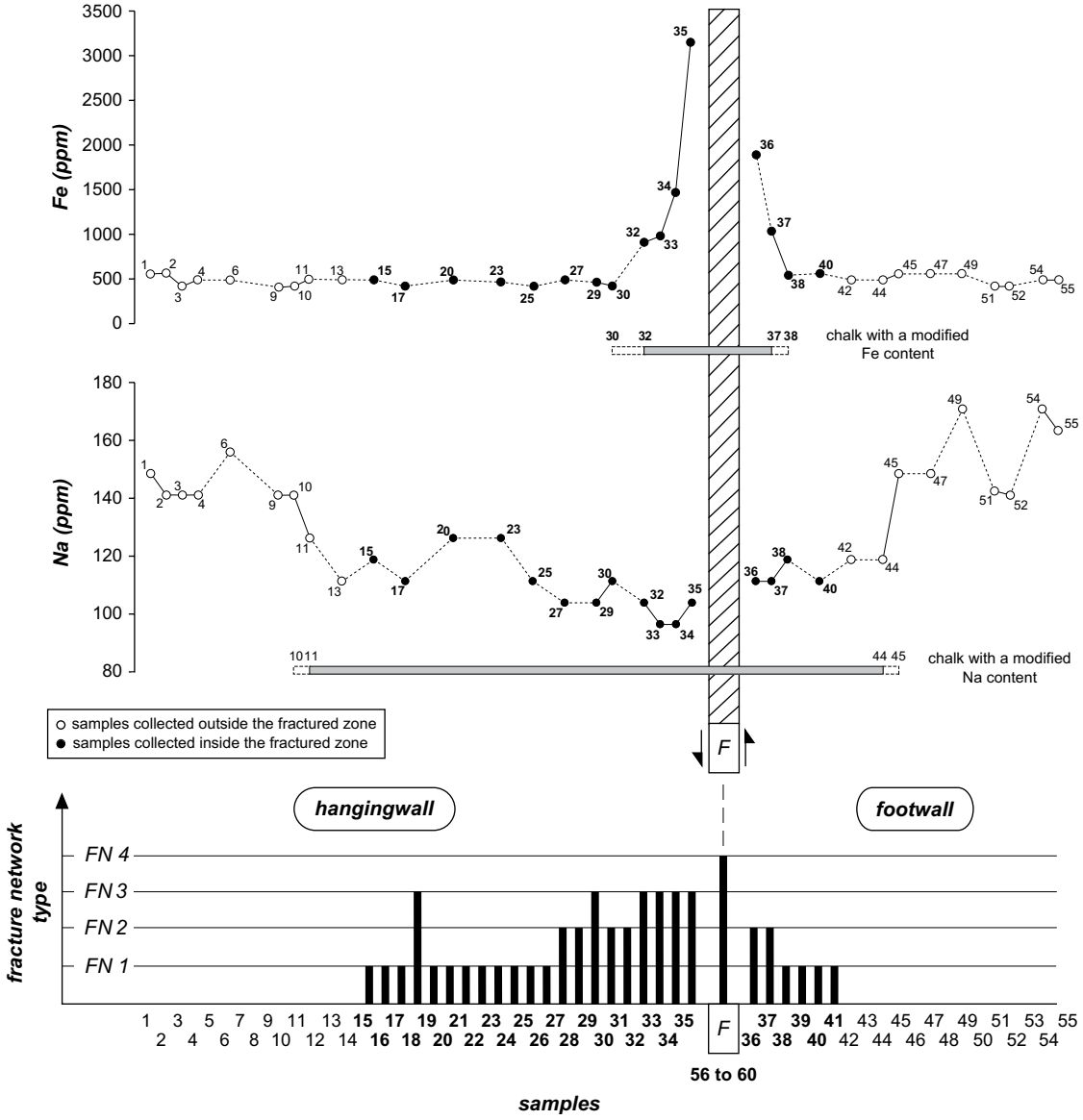

Fig. 5. Evolution of the elemental composition (Fe and Na) of the Coniacian chalk collected in the Marson Quarry along the studied outcrop. The chemical data are plotted by using a constant sampling interval on the *x*-axis.

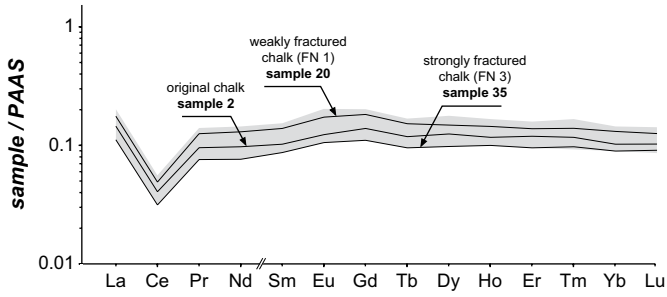

Fig. 6. Rare earth element concentrations (log scale) versus atomic number. The rare earth element contents are normalized to the Post-Archean Australian Average Shale (PAAS) values proposed by McLennan (1989). The grey area indicates the range of rare earth element contents. The black lines represent the rare earth element patterns of samples 2 (original chalk), 20 (weakly fractured chalk, FN 1) and 35 (strongly fractured chalk, FN 3).

4.1.3. Geochemical delimitation of the deformed zone

The geochemical data reveal that the most sensitive markers of the deformation are Sr and Al (Al displays the same variations as K, Rb, Si, Ta, Th, Y and rare earth elements). Sr and Al contents indicate that the development of the fractured zone induced modifications within a 30.2 ± 3.5 m wide zone (samples 9–10 to 45–47, Fig. 4). This geochemically modified zone is wider than the fractured zone (11.4 m, samples 15 to 41) and it is wider in the hangingwall (17.5 ± 1.5 m, samples 9–10 to 35) than in the footwall (12.7 ± 2 m, samples 36 to 45–47). But the ratio W_{GZ}/W_{FZ} (W_{GZ}: geochemically modified zone width, W_{FZ}: fractured zone width) is higher in the footwall (12.7 ± 2 m/1.1 m = 9.7–13.4) than in the hangingwall (17.5 ± 1.5 m/10.3 m = 1.55–1.85). The geochemically modified zone outside the fractured zone is wider in the footwall (11.6 ± 2 m, samples 41 to 45–47) than in the hangingwall (7.2 ± 1.5 m, samples 9–10 to 15).

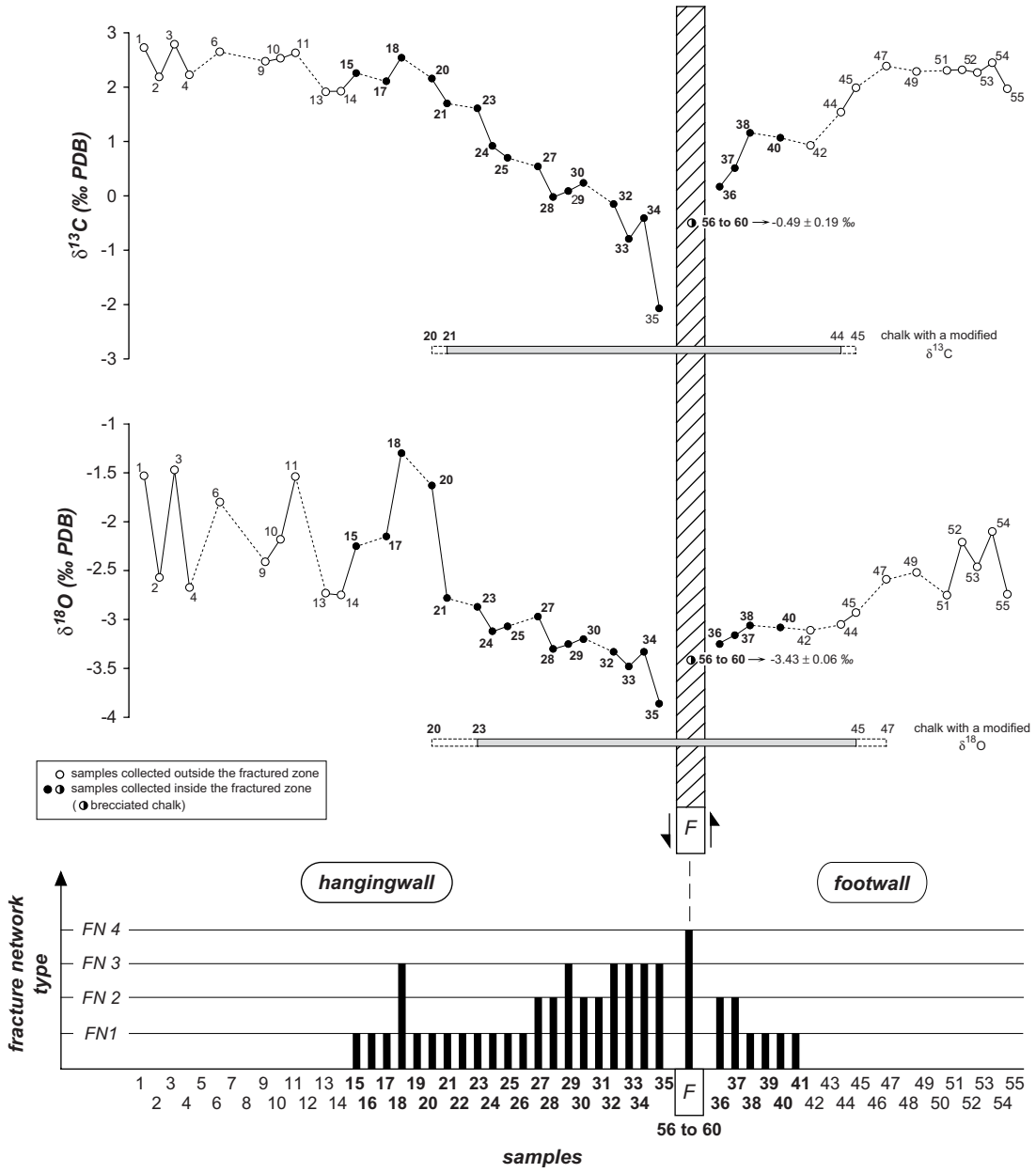

Fig. 7. Evolution of the isotopic composition ($\delta^{18}O$ and $\delta^{13}C$) of the Coniacian chalk collected in the Marson Quarry along the studied outcrop. The isotopic data are plotted by using a constant sampling interval on the *x*-axis.

4.2. Mass and volume changes

4.2.1. Identification of immobile elements

In order to quantify the changes in mass and volume due to the deformation by using the isocon method, immobile elements must be first identified (Grant, 2005). Some evidence suggests that Al, K, Rb, Si, Ta, Th, Y and rare earth elements are insoluble residue proxies in the Coniacian chalk from the Omey area and that they can be reasonably considered as immobile elements during the deformation:

- It is established that Al, Si, K and rare earth elements can be considered as insoluble residue proxies in chalk (Jarvis, 1980, 1992; Wray, 1995; Jarvis et al., 2001; Pearce et al., 2003). The Coniacian chalk from the Omey area is a "white chalk" with an insoluble residue below 2.5%. Its clay association mainly consists of illite, smectite and kaolinite (Labourguigne and Mégnien, 1975). Considering the characteristics of the diagenetic environment during the deformation in the Omey area (Coulon and Frizon de Lamotte, 1988b; Richard et al., 1999), especially the depth (from −150 to −250 m) and the temperature (below 50 °C), it is reasonable to consider that the clay association of the Coniacian chalk was protected from significant diagenetic effects (Chamley, 1989; Weaver, 1989; Bergaya et al., 2006).
- The Al and Sr behaviours are different (Fig. 4). The Sr behaviour is due to the dissolution of primary (marine) carbonate phases and the precipitation of secondary carbonate phases in presence of meteoric porewaters (Richard et al., 2002).
- The rare earth element pattern (Fig. 6) does not show significant modifications caused by the deformation (Section 4.1.1).
- The observations in polarized light microscopy, cathodoluminescence microscopy and SEM show that no evidence of dissolution and/or precipitation of silica is observed in the chalk or in the syntectonic cements filling the normal fault and the tension gashes of the studied outcrop.
- The correlation matrix from the normalised principal component analysis of the chemical data-set indicates that Al, K, Rb, Si, Ta, Th, Y and rare earth elements are strongly correlated. This positive correlation reveals that these elements shared the same behaviour during the deformation.

4.2.2. Analytical data used

The changes in mass and volume (Fig. 8) were quantified by using the Al content because the normalized principal component analysis of immobile element concentrations (Al, K, Rb, Si, Ta, Th, Y and rare earth elements) shows that Al has the highest mean correlation coefficient (0.964).

In order to calculate the changes in mass and volume due to the deformation, the equations (6) and (7) were applied (Section 3.2):

$$V^{O}/V^{A} = \left(C_i^{A}/C_i^{O}\right)\ \left(\rho^{A}/\rho^{O}\right) \tag{6}$$

$$M^{O}/M^{A} = \left(\rho^{O}/\rho^{A}\right)\ \left(V^{O}/V^{A}\right) = C_i^{A}/C_i^{O} \tag{7}$$

To use the equations (6) and (7), it is necessary to determinate the Al concentrations in the original and altered rock (C_i^{O} and C_i^{A} respectively) and the corresponding bulk densities (ρ^{O} and ρ^{A}). The examination of the Al concentration versus sample position curve (Section 4.1.1) allows definition and comparison of the Al signature of the original chalk from the hangingwall and the footwall (Table 1). The original chalk from the hangingwall and the footwall shows two different Al signatures (Table 1) linked to a chemostratigraphic variability. So the hangingwall and the footwall were studied by using two different reference values (Table 1). The samples used to calculate the reference values C_i^{O} do not show evidence of petrophysical modifications due to the deformation (Richard et al., 2002). Therefore C_i^{O} and ρ^{O} were calculated by using the same samples (Table 1).

4.2.3. Quantification and spatial distribution of mass and volume changes

In the hangingwall, two diagenetic evolution types (A and B) can be distinguished (Fig. 8). Type A is observed in samples 10, 11, 13, 15, 20 and 23. It is characterized by mass and volume losses which reach respectively 36% and 35% (highest values, sample 23). The mass and volume changes are very close with a maximal difference of 4% (Fig. 9). Type B (samples 25, 27, 29, 30 and 32 to 35) is characterized by mass gains without volume change. The highest mass gain reaches 58% (sample 35). In the hangingwall, the diagenetic evolutions of type A and type B show a spatial distribution. Type A is observed within an external zone where the chalk is not or weakly (FN 1) fractured while type B is located within an internal zone where the chalk is weakly (FN 1) to strongly (FN 3) fractured (Fig. 8). Sample 17 exhibits a distinct diagenetic evolution related to the development of a type 3 fracture network (sample 18) within a wide zone where the chalk is not or weakly (FN 1) fractured. It probably represents the result of an intermediate diagenetic evolution between the types A and B.

The type A and type B diagenetic evolutions are also recognized in the footwall (Fig. 8): sample 45 shows a type A while samples 36, 38, 40 and 42 exhibit a type B. The mass or volume gains and losses are similar to those observed in the hangingwall but, in the footwall, type A is only observed outside the fractured zone and type B is recognized within an internal zone where the chalk is not or weakly (FN 1) to moderately (FN 2) fractured. Sample 44 probably represents an intermediate diagenetic evolution between the types A and B.

4.2.4. Comparison with previous works

A previous study (Richard et al., 2002) allowed to distinguish two diagenetic evolutions by using the bulk density (ρ) of chalk and the percentage (x) of secondary calcite (calcite precipitated in chalk during the deformation) calculated with the Sr concentrations (Fig. 10A). One of these diagenetic evolutions is characterized by a secondary calcite precipitation without any change in dry density. The other shows a secondary calcite precipitation and an increase in dry density. The comparison of results of this previous study with the mass and volume changes (Fig. 10A,B) reveals that:

- Type A diagenetic evolution is observed where the deformation caused a secondary calcite precipitation without any change in dry density. No change in dry density involves equal changes in mass and volume: the mass and volume changes observed for the type A diagenetic evolution are very close, the difference never exceed 4% (Section 4.2.3). These diagenetic modifications are in agreement with an increase in insoluble residue.
- Type B diagenetic evolution is observed where the deformation induced a secondary calcite precipitation associated with an increase in dry density. An increase in dry density is in agreement with a mass gain without volume change and a decrease in insoluble residue.

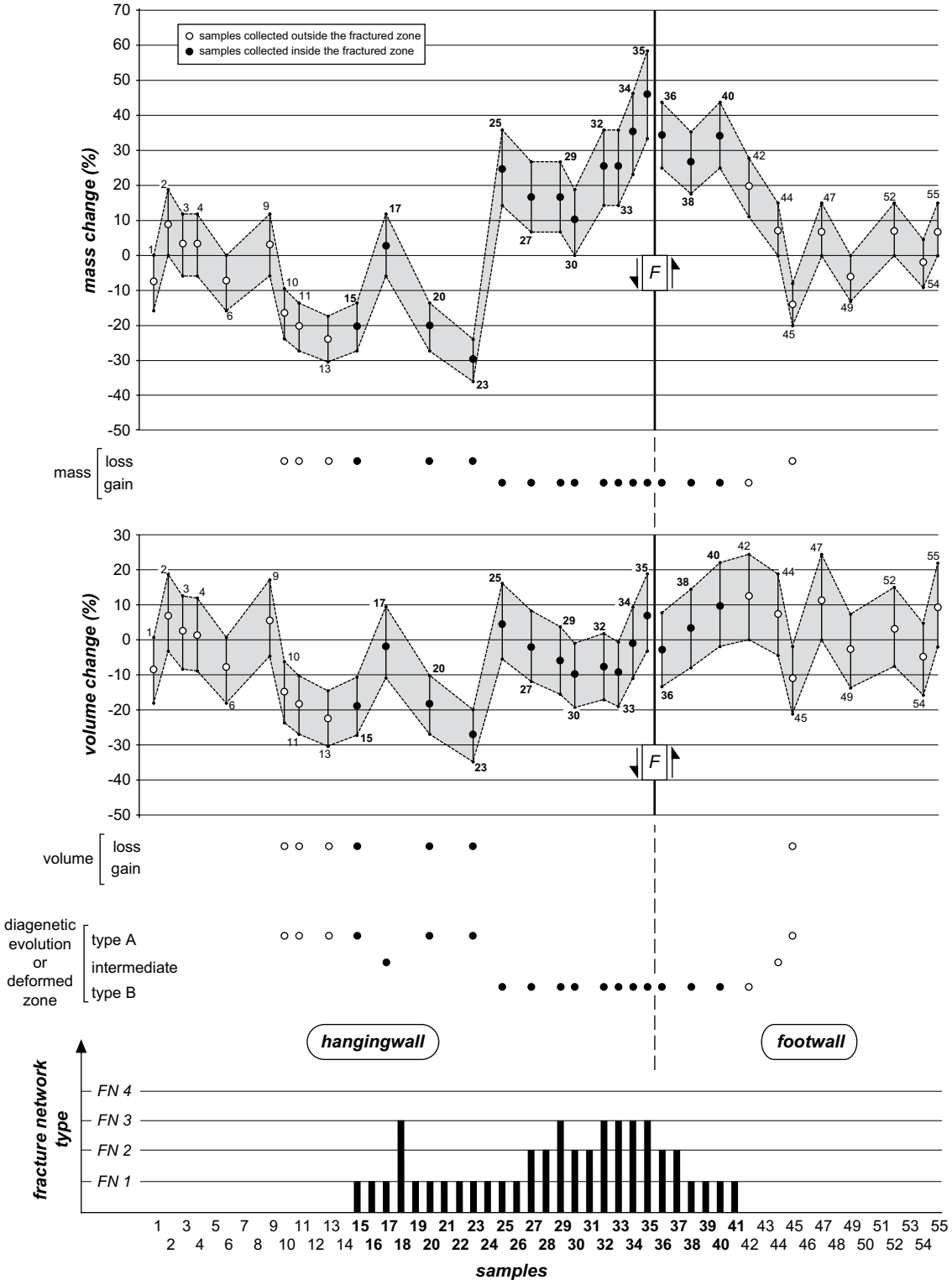

Fig. 8. Mass and volume changes caused by the development of one normal fault and related tension gashes in the Coniacian chalk from the Marson Quarry. Two diagenetic evolution types can be distinguished: type A characterized by equal mass and volume losses and type B showing mass gains without volume change. The range of changes in mass and volume (grey area) is due to the range of Al content and bulk density of the original chalk (respectively C_i^O and ρ^O in equations (6) and (7), Section 4.2.2). The circles indicate the mass and volume changes calculated by using the mean values of Al content and bulk density of the original chalk.

Table 1
Al signature of the original chalk (C_i) from the hangingwall and the footwall and corresponding bulk densities (ρ^O)

	Al		Bulk density	
	Hangingwall	Footwall	Hangingwall	Footwall
Samples	1, 2, 3, 4, 6, 9	47, 49, 52, 54, 55	1, 2, 3, 4, 6, 9	47, 49, 52, 54, 55
Minimum value	847 ppm	1058 ppm	1.574	1.510
Maximum value	1006 ppm	1217 ppm	1.628	1.633
Range	159 ppm	159 ppm	0.054	0.123
Mean	926 ppm	1111 ppm	1.609	1.567
Reference values	847/1006 ppm	1058/1217 ppm	1.574/1.628	1.510/1.633

– The deformed zones recognized with these two approaches are the same (from samples 9–10 to 45–47).

Previous petrophysical measurements and SEM observations (Richard et al., 2002) compared with the mass and volume changes (Fig. 10B–D) indicate that:

– type A diagenetic evolution displays an increase in *kh* (permeability × capillary suction) and pore access diameters without any change in chalk fabric, particle contacts, propagation velocity of longitudinal ultrasonic waves, total porosity and trapped porosity (Fig. 10B, C, sample 20);
– type B diagenetic evolution shows a change in chalk fabric and particle contacts (important increase in solid–solid contacts), a decrease in total porosity, *kh* and pore access diameters and an increase in trapped porosity and propagation velocity of longitudinal ultrasonic waves (Fig. 10B, C, samples 31 and 35).

A comparison between the percentages (x) of secondary calcite calculated with the Sr contents (Richard et al., 2002) and the mass gains and losses shows that:

– precipitation occurred in chalk showing a diagenetic evolution of type A despite the mass losses: for example, the percentage of secondary calcite of sample 15 varies from 13% to 25% while the mass loss ranges between 14% and 27%;
– dissolution occurred in chalk showing a diagenetic evolution of type B despite the mass gains: for example, the mass of secondary calcite of sample 35 ranges between 58 g and 81 g (for an original mass = 100 g) while the mass gain varies from 33 g to 57 g.

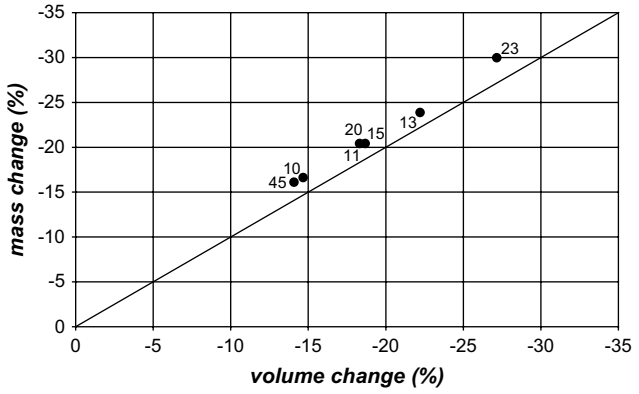

Fig. 9. Comparison between the mass and volume changes in samples showing a type A diagenetic evolution. The mass and volume changes are very close with a maximal difference of 4%. The mass and volume changes were calculated by using the mean values of Al content and bulk density of the original chalk.

5. Interpretation and discussion

5.1. Mass changes

In the studied natural system, the mass gains are observed within the type B deformed zones adjacent to the fault plane while the mass losses are observed within the outermost deformed zones (type A deformed zones) neighbouring the type B deformed zones (Section 4.2.3, Fig. 8). What are the mechanisms operating in these mass changes?

The precipitation of secondary calcite induced by the deformation was quantified by using the Sr contents (Richard et al., 2002). The results of this quantification compared with the mass gains and losses (Section 4.2.4) reveal that precipitation took place within the type A deformed zones despite the mass losses and that dissolution occurred within the type B deformed zones despite the mass gains. According to the physico-chemical model of the deformation mechanism recognized for this natural system (Richard et al., 2002), it appears that:

– Within the type A deformed zones, precipitation probably occurred at the solid-fluid contacts (free faces of particles) when the interstitial fluids were supersaturated with respect to calcite (Fig. 11).
– Within the type B deformed zones, dissolution probably took place at the solid-fluid contacts during the undersaturated fluid inputs (Fig. 11). This dissolution was restricted by the decrease in total porosity and transport properties recognized in the chalk of the type B deformed zones (Section 4.2.4). The mass gains without volume change observed within the type B deformed zones imply that there was no dissolution along the solid–solid contacts (particle contacts) by increase in normal stresses and at the margins of solid–solid contacts by increase in plastic or elastic energy (Fig. 11).

It follows that precipitation and dissolution occurred within the deformed zones of types A and B, but this study clearly indicates that the ratio dissolution/precipitation is above 1 within the type A deformed zones and below 1 within the type B deformed zones (Fig. 11). The petrophysical and SEM characteristics of the chalk of the deformed zones of types A and B (Section 4.2.4) allow explanation of this phenomenon. Within the type B deformed zones, the particles are under lower stress–strain energy than within the type A deformed zones. This lower stress–strain energy within the type B deformed zones is linked to more important particle contacts. Dissolution preferentially thus took place within the most porous zones (type A deformed zones) with a positive feedback relationship between the total porosity and dissolution (Merino et al., 1983; Merino, 1992) and precipitation preferentially occurred within the least porous zones (type B deformed zones). It is reasonable to consider that the mass gains and losses described in this study correspond to a mass redistribution from the most to the least porous zones (Fig. 11). Chalk of the type A deformed zones shows the highest transport properties (highest *kh* and pore access diameter, Fig. 10C). A positive feedback relationship between the transport properties and dissolution probably operated within the type A deformed zones: a faster interstitial fluid flow through the medium promotes faster local dissolution (Ortoleva et al., 1987a,b).

The comparison between the results of the present study and the SEM observations (Fig. 10B–D) shows that, at the grain scale, the mass gains promoted an overgrowth of particles with a change in shape (from regular to irregular) and morphology (from anhedral to subhedral/euhedral), a modification in particle contacts (from point-contacts to straight or curved compromise contacts) and an increase in the amount of secondary particles

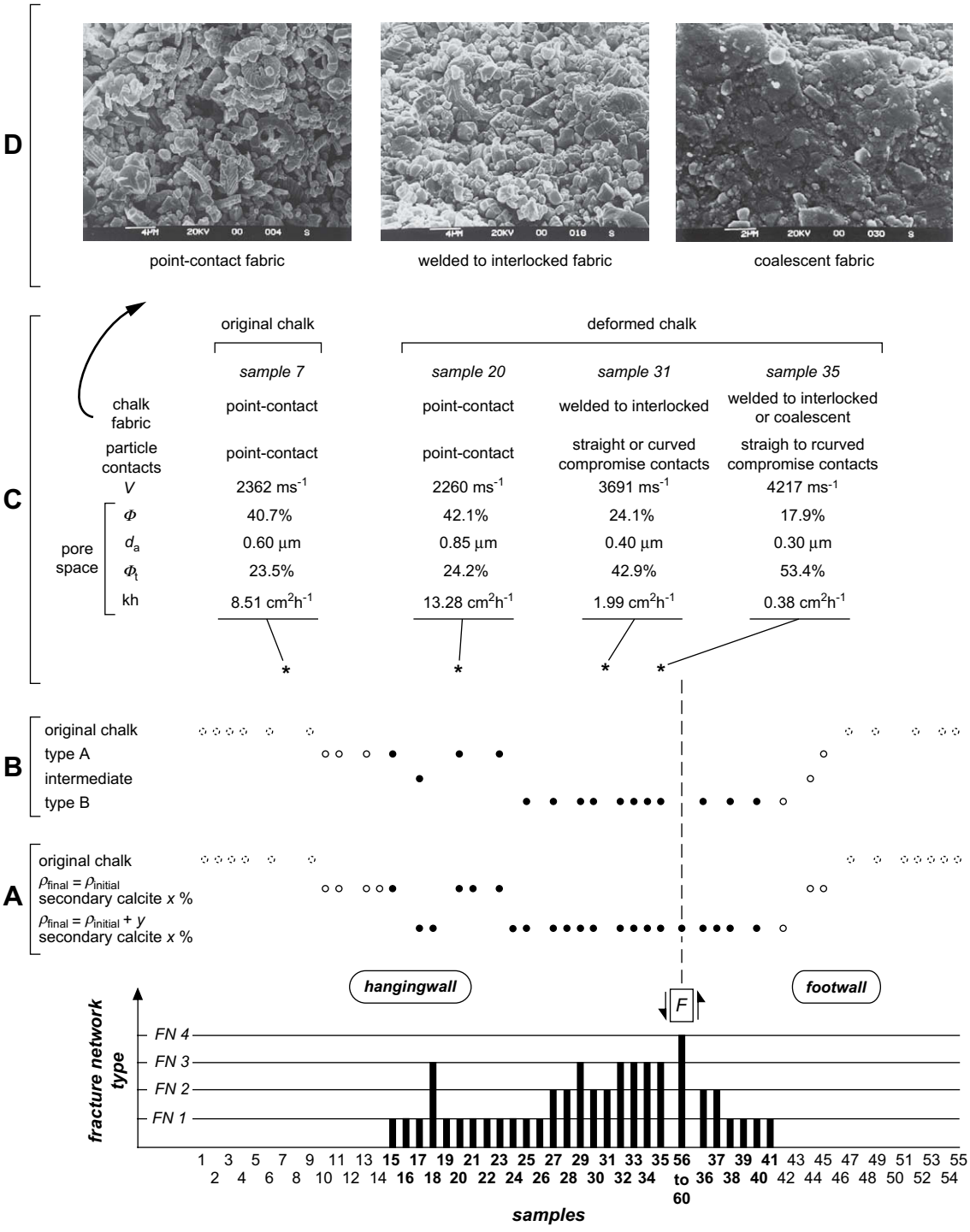

Fig. 10. Diagenetic evolutions caused by the development of one normal fault and related tension gashes in the Coniacian chalk from the Marson Quarry. (A) Diagenetic evolutions distinguished by using the bulk density (ρ) of chalk and the percentage (x) of secondary calcite (Richard et al., 2002). (B) Diagenetic evolutions distinguished by using the mass and volume changes (this study). (C) Chalk fabric, particle contacts, propagation velocity of longitudinal ultrasonic waves (V), pore space (Φ = total porosity, d_a = pore access diameter, Φ_t = trapped porosity, kh = permeability k × capillary suction h) of the original and deformed chalk (Richard et al., 2002). (D) Views of fabrics of the original and deformed chalk.

Fig. 11. Physico-chemical model of the deformation mechanism of the Coniacian chalk from the Marson Quarry. In the Omey area, the Oligocene extension led to the development of normal faults and tension gashes in an unconfined phreatic zone (between −150 and −250 m) where the interstitial fluid was meteoric. The development of these fractures induced through time temporary decreases in interstitial fluid pressure and flows of porewaters through chalk to active fractures. Each decrease in interstitial fluid pressure led first an input of undersaturated fluids with respect to calcite (t_1). During this stage, dissolution occurred within the type A deformed zones, along the solid–solid contacts (particle contacts) by increase in normal stresses, at the margins of the solid–solid contacts by increase in plastic or elastic energy and at the solid-fluid contacts (free faces of particles). Within the type B deformed zones, dissolution took place at the solid fluid-contacts. Each decrease in interstitial fluid pressure involved secondly the flow of supersaturated fluids with respect to calcite (t_2). During this stage, dissolution continued along the solid–solid contacts within the type A deformed zones and precipitation took place at the solid-fluid contacts within the deformed zones of types A and B. A positive feedback relationship between the transport properties and dissolution probably operated within the type A deformed zones. The percentage of secondary calcite (calcite precipitated in chalk during the deformation at the free faces of particles) calculated with the Sr concentrations ranges between 12% and 24% within the type A deformed zones and between 21% and 47% within the type B deformed zones. The ratio dissolution/precipitation is above 1 within the type A deformed zones and below 1 within the type B deformed zones. A mass redistribution took place from the most porous zones (outermost deformed zones) to the least porous zones (deformed zones adjacent to the fault). These mass transfers induced volume losses within the type A deformed zones where chemical compaction occurred in response to the reduction in solid–solid contacts.

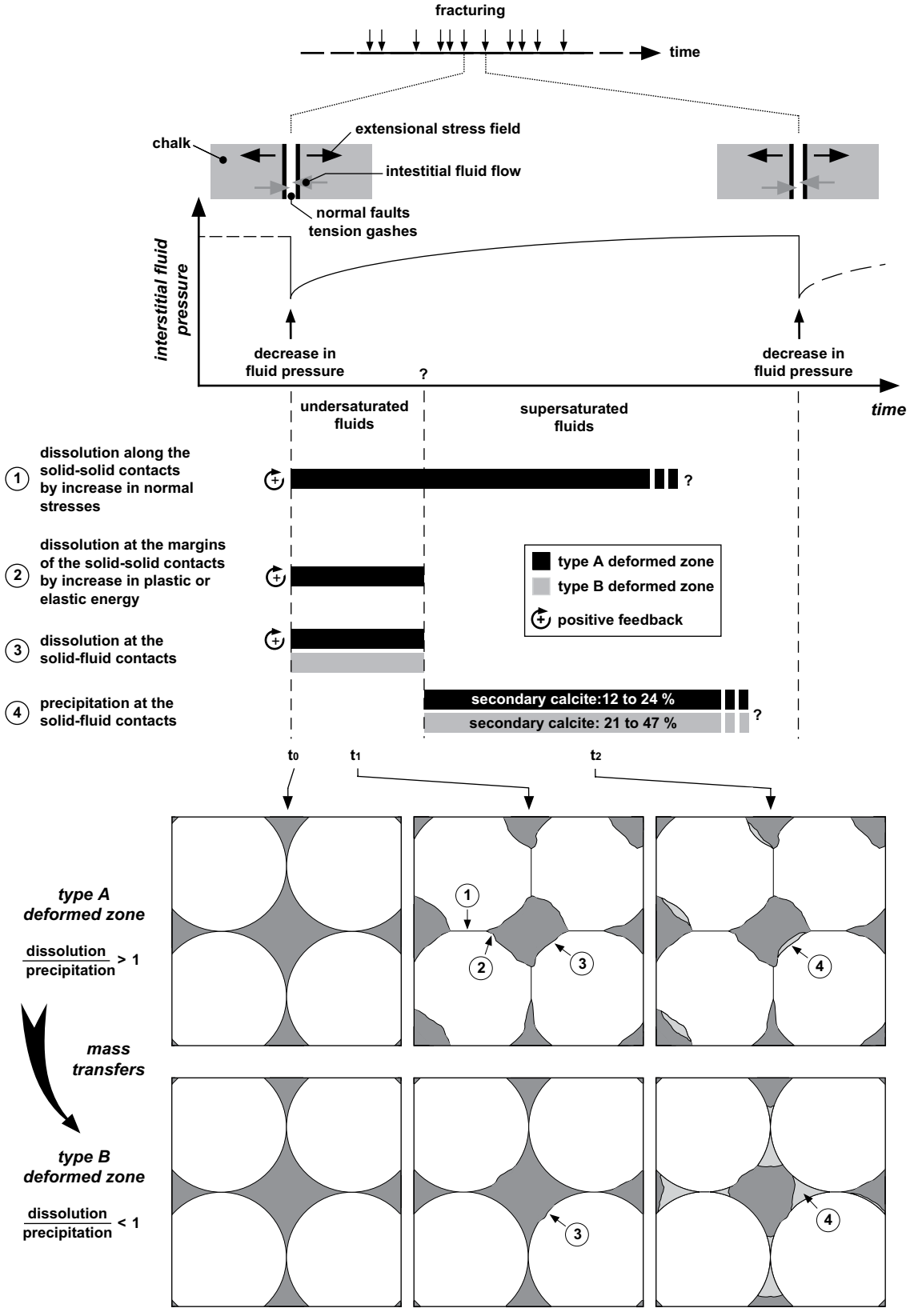
fracturing
time
chalk
extensional stress field
intestitial fluid flow
normal faults
tension gashes
interstitial fluid pressure
decrease in fluid pressure
decrease in fluid pressure
?
undersaturated fluids
supersaturated fluids
time
1 dissolution along the solid-solid contacts by increase in normal stresses
2 dissolution at the margins of the solid-solid contacts by increase in plastic or elastic energy
3 dissolution at the solid-fluid contacts
4 precipitation at the solid-fluid contacts
type A deformed zone
type B deformed zone
positive feedback
secondary calcite:12 to 24 %
secondary calcite: 21 to 47 %
?
t0
t1
t2
type A deformed zone
dissolution / precipitation > 1
mass transfers
type B deformed zone
dissolution / precipitation < 1

related to cementation of coccolith fragments and/or primary particles. The nucleation of new crystals is scarce. Dissolution pits at the free faces of particles, notably at the rim of pores, is the only evidence for mass losses. The SEM observations also show that the chalk fabric within the deformed zones of types A and B is not uniform: one sample always displays several fabrics (point-contact, welded, interlocked and/or coalescent). The mass gains and losses do not therefore appear uniform within the chalk at the grain scale.

5.2. Volume changes

No volume change is observed within the type B deformed zones while the type A deformed zones show significant volume losses (Section 4.2.3, Fig. 8). An explanation can be proposed by considering the SEM and petrophysical characteristics of the deformed zones of types A and B (Section 4.2.4, Fig. 10) and the physico-chemical model proposed for this natural system (Fig. 11). Within the type A deformed zones, dissolution occurred along the solid–solid contacts by increase in normal stresses and at the margins of the solid–solid contacts by increase in plastic or elastic energy (Fig. 11). A chemical compaction therefore took place in response to these mass losses. Conversely, within the type B deformed zones, the mass gains promoted an increase in solid–solid contacts that inhibited the chemical compaction. Within the type A deformed zones, no evidence suggests that the chemical compaction is more intense in particular zones.

5.3. Relationships between mass and volume changes and fracturing

At first sight, it appears that the type A deformed zones are observed where the chalk is not or weakly fractured and that the type B deformed zones are localized within the most fractured zones (Fig. 8). But a more detailed examination of data allows refinement of this conclusion:

- The spatial distribution of type B deformed zones (and consequently the spatial distribution of type A deformed zones) is strongly controlled by the distance to the fault plane because (1) in the hangingwall and the footwall, the type B deformed zones are adjacent to the fault plane and (2) in the footwall, the mass gains are equal to those observed within the hangingwall though the chalk is not or weakly fractured (Fig. 8). This case study did not allow to fully clarify the control of tension gashes on the mass transfers. Nevertheless, it appears that they played a significant role because (1) they induced, like the fault, temporary decreases in interstitial fluid pressure which promoted and activated the deformation mechanism (Richard et al., 1999, 2002; Fig. 11), (2) the field observations show that the development of tension gash networks without fault promoted a chalk deformation with mass transfers, and (3) sample 17 indicates that the development of a type 3 fracture network within a type A deformed zone inhibited the related mass and volume losses (Fig. 8).
- The development of tension gashes restricts the diagenetic impact of the fault when it reaches a threshold (probably between FN 2 and 3): the type B deformed zone is wider in the footwall (5.7 ± 2 m) than in the hangingwall (2.9 ± 1.3 m) though fracturing is more important in the hangingwall (FN 1–3, mainly FN 2 and 3) than in the footwall (not fractured to FN 2, mainly FN 1). The reduction of the diagenetic impact of the fault results from a partition of the medium which probably induced a decrease in temporary flows of porewaters through pore space due to the fault activity (notably in the hangingwall).

The strong control of the spatial distribution of the deformed zones of types A and B by the distance to the fault plane and the restriction of the diagenetic impact of the normal fault induced by the development of tension gashes explain that:

- the ratio W_{GZ}/W_{FZ} (W_{GZ}: geochemically modified zone width, W_{FZ}: fractured zone width) is higher in the footwall (12.7 ± 2 m/1.1 m = 9.7–13.4) than in the hangingwall (17.5 ± 1.5 m/10.3 m = 1.55–1.85);
- the geochemically modified zone outside the fractured zone is wider in the footwall (11.6 ± 2 m, samples 41 to 45–47) than in the hangingwall (7.2 ± 1.5 m, samples 9–10 to 15).

6. Conclusions

The present contribution highlights that the interactions between pressure solution and fracturing processes can induce important mass transfers and volume changes in carbonate rocks. The mass and volume changes caused by the development of one normal fault and related tension gashes occur in the hangingwall as well as in the footwall. These mass and volume changes show a spatial distribution: the deformed zones adjacent to the fault plane exhibit mass gains without volume changes while the outermost deformed zones display equal mass and volume losses. This spatial distribution is strongly controlled by the distance to the fault plane but the tension gashes probably play a significant role. They notably restrict the diagenetic impact of the fault by partitioning the medium. The mass changes result from mass transfers from the most porous zones (outer deformed zones) to the least porous zones (deformed zones adjacent to the fault) due to differences in stress–strain energy of grain aggregates. Pressure solution operates with a negative feedback relationship between the solid–solid contacts and dissolution and a positive feedback relationship between the transport properties and dissolution. At the grain scale, the mass gains and losses do not appear uniform within chalk. The mass transfers induce volume losses within the outermost deformed zones where chemical compaction takes place in response to the reduction in solid–solid contacts.

Acknowledgements

I would like to thank Dr. R.E. Holdsworth, Dr. J.P. Gratier and an anonymous reviewer for their extensive and constructive comments that led to substantial improvements of the manuscript. I am grateful to O. Fabbri for his comments and English proofreading.

References

Angelier, J., Vandycke, S., Bergerat, F., Gaviglio, P., Schroeder, C., Coulon, M., 2006. Can belemnite distribution reveal pressure-solution processes along faults? A case study in chalk of the Mons Basin, Belgium. Journal of Structural Geology 28, 64–82.

Bergaya, F., Theng, B.K.G., Lagaly, G., 2006. Handbook of clay science. In: Developments in Clay Science 1. Elsevier. 1141-1149.

Bergerat, F., 1987a. Stress fields in the European platform at the time of Africa-Eurasia collision. Tectonics 6, 99–132.

Bergerat, F., 1987b. Paléo-champs de contrainte tertiaires dans la plate-forme européenne au front de l'orogenèse alpin. Bulletin de la Société Géologique de France 3, 611–620.

Carrio-Schaffhauser, E., Gaviglio, P., 1990. Pressure solution and cementation stimulated by faulting in limestones. Journal of Structural Geology 12, 987–994.
Chamley, H., 1989. Clay Sedimentology. Springer, Berlin, pp. 333-358.
Coulon, M., 1992. La distension oligocène dans le nord-est du Bassin de Paris (perturbation des directions d'extension et distribution des stylolites). Bulletin de la Société Géologique de France 5, 531–540.
Coulon, M., Frizon de Lamotte, D., 1988a. Les extensions cénozoïques dans l'est du Bassin de Paris: mise en évidence et interprétation. Comptes rendus de l'Académie des Sciences II 307, 1113–1119.
Coulon, M., Frizon de Lamotte, D., 1988b. Les craies éclatées du secteur d'Omey (Marne, France): le résultat d'une bréchification par fracturation hydraulique en contexte extensive. Bulletin de la Société Géologique de France 1, 177–185.
Gaviglio, P., Chaye d'Albissin, M., Bergerat, F., Vandycke, S., 1993. Modifications de texture dans la craie au contact de failles normales: un exemple de graben dans le bassin de Mons (Belgique). Bulletin de la Société Géologique de France 4, 565–575.
Gaviglio, P., Adler, P., Thovert, J.F., Vandycke, S., Bergerat, F., Bekri, S., Lestideau, R., 1997. Grain-scale microstructures and physical properties of faulted chalk. Bulletin de la Société Géologique de France 6, 727–739.
Gaviglio, P., Vandycke, S., Schroeder, C., Coulon, M., Bergerat, F., Dubois, C., Pointeau, I., 1999. Matrix strains along normal fault planes in the Campanian White Chalk of Belgium: structural consequences. Tectonophysics 309, 41–56.
Grant, J.A., 1986. The isocon diagram—a simple solution to Gresens' equation for metasomatic alteration. Economic Geology 81, 1976–1982.
Grant, J.A., 2005. Isocon analysis: a brief review of the method and applications. Physics and Chemistry of the Earth 30, 997–1004.
Gratier, J.P., Renard, F., Labaume, P., 1999. How pressure solution creep and fracturing processes interact in the upper crust to make it behave in both a brittle and viscous manner. Journal of Structural Geology 21, 1189–1197.
Gresens, R.L., 1967. Composition–volume relationships of metasomatism. Chemical Geology 2, 47–65.
Hellmann, R., Renders, P.J.N., Gratier, J.P., Guiguet, R., 2002. Experimental pressure solution compaction of chalk in aqueous solutions. Part 1. Deformation behavior and chemistry. In: Hellmann, R., Wood, S.A. (Eds.), Water–Rock Interactions, Ore Deposits, and Environmental Geochemistry. Special Publications, no. 7. The Geochemical Society, pp. 129–152.
Hellmann, R., Gaviglio, P., Renders, P.J.N., Gratier, J.P., Békri, S., Adler, P., 2002b. Experimental pressure solution compaction of chalk in aqueous solutions. Part 2. Deformation examined by SEM, porosimetry, synthesis permeability and X-ray computerized tomography. In: Hellmann, R., Wood, S.A. (Eds.), Water–Rock Interactions, Ore Deposits, and Environmental Geochemistry. Special Publications, no. 7. The Geochemical Society, pp. 153–178.
Jarvis, I., 1980. Geochemistry of phosphatic chalks and hardgrounds from the Santonian to early Campanian (Cretaceous) of northern France. Journal of the Geological Society, London 137. 705-721.
Jarvis, I., 1992. Sedimentology, geochemistry and origin of phosphatic chalks: the Upper Cretaceous deposits of NW Europe. Sedimentology 39, 55–97.
Jarvis, I., Murphy, A.M., Gale, A.S., 2001. Geochemistry of pelagic and hemipelagic carbonates: criteria for identifying systems tracts and sea-level change. Journal of the Geological Society, London 158. 685-696.
Jones, M.E., Bedford, J., Clayton, C., 1984. On natural deformation mechanisms in the chalk. Journal of the Geological Society, London 141. 675-683.
Labourguigne, J., Mégnien, F., 1975. Notice explicative de la carte géologique de la France à 1/50 000 de Châlons-sur-Marne (no. 189). Bureau de Recherches Géologiques et Minières, Orléans 10.
McLennan, S.M., 1989. Rare earth elements in sedimentary rocks: influence of provenance and sedimentary processes. In: Lipin, B.R., McKay, G.A. (Eds.), Geochemistry and Mineralogy of Rare Earth Elements. Reviews in Mineralogy 21. Mineralogical Society of America, pp. 169–200.
Merino, E., 1992. Self-organization in stylolites. American Scientist 80, 466–473.
Merino, E., Ortoleva, P., Strickholm, P., 1983. Generation of evenly-spaced pressure-solution seams during (late) diagenesis: a kinetic theory. Contributions to Mineralogy and Petrology 82, 360–370.
Mimran, Y., 1975. Fabric deformation induced in Cretaceous chalks by tectonic stresses. Tectonophysics 26, 309–316.
Mimran, Y., 1977. Chalk deformation and large-scale migration of calcium carbonate. Sedimentology 24, 333–360.
Ortoleva, P., Chadam, J., Merino, E., Sen, A., 1987a. Geochemical self-organization II: the reactive-infiltration instability. American Journal of Science 287, 1008–1040.
Ortoleva, P., Merino, E., Moore, C., Chadam, J., 1987b. Geochemical self-organization I: reaction-transport feedbacks and modelling approach. American Journal of Science 287, 979–1007.
Pearce, M.A., Jarvis, I., Swan, A.R.H., Murphy, A.M., Tocher, B.A., Edmunds, W.M., 2003. Integrating palynological and geochemical data in a new approach to palaeoecological studies: Upper Cretaceous of the Banterwick Barn Chalk borehole, Berkshire, UK. Marine Micropaleontology 47, 271–306.
Richard, J., Coulon, M., Gaviglio, P., Ramseyer, K., 1997. L'hydrofracturation: une deformation tectonique à haut potentiel diagénétique. Exemple des craies hydrofracturées de la region d'Omey (Bassin de Paris, France). Comptes rendus de l'Académie des Sciences IIA 325, 359–366.
Richard, J., Barbin, V., Ramseyer, K., Pascal, A., Roux, M., Henry, P., 1999. Les ciments syntectoniques: des enregistrements complexes de la diagenèse liée aux déformations tectoniques cassantes. Exemple des ciments des craies hydrofracturées de l'est du bassin de Paris. Bulletin de la Société Géologique de France 5, 719–731.
Richard, J., Coulon, M., Gaviglio, P., 2002. Mass transfer controlled by fracturing in micritic carbonate rocks. Tectonophysics 350, 17–33.
Weaver, C.E., 1989. Clays, Muds, and Shales. In: Developments in Sedimentology, Vol. 44. Elsevier, Amsterdam, pp. 417-449.
Wray, D.S., 1995. Origin of clay-rich beds in Turonian chalks from Lower Saxony, Germany—a rare-earth element study. Chemical Geology 119, 161–173.